tive reactance contributed from the shorting pin and the probe; thus a wider antenna bandwidth could be achieved [4].

The radiation patterns for the compact antenna with $l = d$ are presented in Figure 4. It is seen that the radiation patterns remain broadside. Figure 5 shows the case for the antenna without slots ($l = 0$), where the patch resonates at about 1.923 GHz. Similar broadside radiation is also observed. However, because of the increase of the patch surface current component perpendicular to the main excitation direction [3], the cross-polarization radiation in the H plane is increased (cf. Figures 4 and 5). On the other hand, the cross-polarization level in the E-plane is still in an acceptable level of less than -20 dB. Finally, it should also be noted that, due to the antenna size reduction, the antenna gain of a compact microstrip antenna will be lower than that of a conventional microstrip antenna operated at the same frequency [2].

3. CONCLUSIONS

The design of a compact meandered circular microstrip antenna with a shorting pin has been described. Experimental results have been presented and discussed. Results indicate that, by combining short-circuiting and meandering of the circular patch, the antenna size can be reduced to be less than 10% that of a conventional circular microstrip antenna operated at the same frequency. This great reduction in antenna size makes it useful for applications where antenna size is a major concern.

REFERENCES

1. K. Hiraswa and M. Haneishi, *Analysis, Design, and Measurement of Small and Low-Profile Antennas*, Artech House, London, 1992.
2. R. Waterhouse, "Small Microstrip Patch Antenna," *Electron. Lett.*, Vol. 31, April 13, 1995, pp. 604–605.
3. S. Dey and R. Mittra, "Compact Microstrip Patch Antenna," *Microwave Opt. Technol. Lett.*, Vol. 13, Sept. 1996, pp. 12–14.
4. T. Huynh and K. F. Lee, "Single-Layer Single-Patch Wideband Microstrip Antenna," *Electron. Lett.*, Vol. 31, Aug. 3, 1995, pp. 1310–1312.

CCC 0895-2477/97

AN EQUIVALENT NETWORK METHOD FOR THE ANALYSIS OF NONUNIFORM PERIODIC STRUCTURES

Jin Jei Wu
Institute of Electro-Optical Engineering
National Chiao Tung University
Hsinchu, Taiwan, Republic of China

Received 5 November 1996; revised 10 February 1997

ABSTRACT: *The characteristics of guided waves scattered by nonuniform waveguide gratings are systematically investigated with the use of an equivalent network method. This procedure is based on a combination of the multimode network theory and the rigorous mode-matching method. Concave Bragg gratings and bent waveguide gratings are taken as examples to demonstrate the present approach, and numerical results are given to illustrate their potential for millimeter-wave and optical integrated circuit applications. © 1997 John Wiley & Sons, Inc.* Microwave Opt Technol Lett 15: 149–153, 1997.

Key words: *concave Bragg grating; staircase approximation*

INTRODUCTION

Planar waveguide structures containing a periodic corrugation along the waveguide have long been used for various applications, such as distributed feedback reflectors [1], optical filters, and leaky wave antennas [2]. The electromagnetic problem of a straight uniform periodic structure has been analyzed by various methods, such as the coupled mode theory [1], the finite element method [3], the method of lines [4] and the rigorous mode matching method [2]. With these basic analyses, the properties of Bragg waveguide gratings can be considered to be well understood. In recent years, many authors have conducted work on different types of guided-wave gratings, such as sinusoidal (or triangular) profile gratings and tapered period interval (or profile depth, index contrast, and so on) gratings to improve and tailor the performance of active or passive devices. Thus, it is mandatory to analyze these periodic and aperiodic structures with efficient and accurate numerical methods. The combination of the mode-matching method with multimode network theory has been shown to be very efficient for analyzing the nonuniform dielectric waveguides for integrated optics applications [5]. In this Letter, we will utilize this combined method, which can accurately include both fundamental modes and higher-order modes, to analyze the scattering characteristics of nonuniform waveguide gratings for a millimeter-wave system or for optical integrated circuit applications.

Numerical results presented for different types of nonuniform Bragg gratings, such as concave waveguide gratings and bent waveguide gratings, provide guidelines for optimally designing or improving the performance of optoelectronic devices.

METHOD OF ANALYSIS

As an illustration of this method, consider a two-dimensional structure as depicted in Figure 1(a), which shows a parallel-plate waveguide filled with a concave grating. The scattering of guided waves by nonuniform waveguide gratings (such as concave waveguide gratings and bent waveguide gratings) cannot be analyzed exactly, even though the geometric profile is simple. Thus a useful approximation is needed. We utilize the staircase approximation of the continuous nonuniform profile of the waveguide gratings; this is a discretization in geometry. Figure 1(b) shows the staircase approximation of a concave Bragg grating in the neighborhood of x_i. Therefore, the whole structure can be approximated by a sequence of basic units, each consisting of a waveguide discontinuity and a uniform partially filled parallel-plate waveguide. According to the literature [5], the general field solution in each uniform waveguide region can be expressed in terms of the complete set of mode functions $\{\phi_n\}$, which are the solutions of a Sturm–Liouville eigenvalue problem. For the TE fundamental-mode incident case, the tangential field in each uniform waveguide region can be represented by

$$E_z(x, y) = \sum_n V_n(x)\phi_n(y), \tag{1}$$

$$H_y(x, y) = \sum_n I_n(x)\phi_n(y), \tag{2}$$

where V_n and I_n are the equivalent voltage and current of the nth mode, respectively. By matching the tangential field components at the ith discontinuity, the scattering of modes by a waveguide discontinuity can be quantified by the analysis of

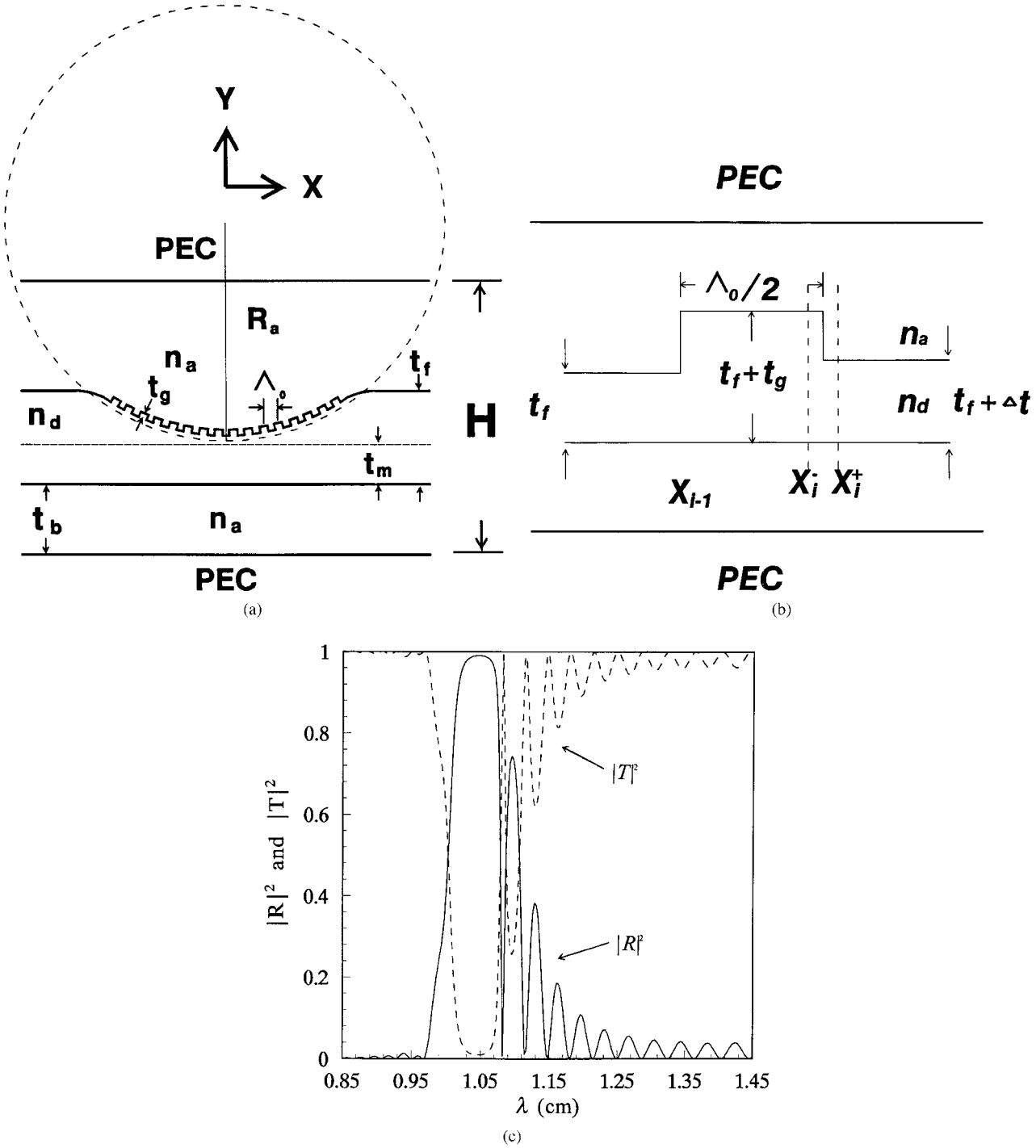

Figure 1 (a) Parallel-plate waveguide filled with concave Bragg gratings. (b) Staircase approximation of a parallel-plate waveguide filled with concave grating. (c) Reflection and transmission spectrum of the fundamental TE mode, for this concave grating with top and bottom cover: $R = 200$ cm, $H = 0.54$ cm, $t_g = 0.045$ cm, $t_b = t_m = 0.09$ cm, $n_d = \sqrt{5}$, $n_a = 1.0$, $\Lambda_0 = 0.36$ cm, and 20 periods

modal currents and voltages. For the voltages and currents on the two sides of the ith step, we obtain the linear systems:

$$V_m(x_i^-) = \sum_n (Q_i)_{mn} V_n(x_i^+), \tag{3}$$

$$I_m(x_i^-) = \sum_n (Q_i)_{mn} I_n(x_i^+), \tag{4}$$

where $(Q_i)_{mn}$ is an element of the coupling matrix at the ith step discontinuity between uniform waveguides. The elements of this matrix can be defined as the scalar products of the mode functions on the two sides of this discontinuity, as follows:

$$(Q_i)_{mn} = \langle \phi_m(x_i^-) \mid \phi_n(x_i^+) \rangle. \tag{5}$$

Note that

$$(Q_i^{-1})_{mn} = (Q_i)_{mn}, \qquad \text{so that } Q_i^{-1} = Q_i^t,$$

where t stands for transposed.

From (5)–(7) it can be easily deduced that the input impedance matrix $Z(x_i^-)$ at the $x = x_i^-$ plane looking to the right satisfies

$$Z(x_i^-) = Q_i(Z(x_i^+))Q_i^t, \tag{6}$$

where the Q matrix is previously defined. From the impedance transform matrix formula (6) the reflection coefficient matrix $\Gamma(x_i^-)$ at the $x = x_i^-$ plane and the impedance matrix $Z(x_{i-1}^+)$ at the $x = x_{i-1}^+$ plane looking to the right can be obtained as

$$\Gamma(x_i^-) = [Z(x_i^-) + Z_{oi}]^{-1}[Z(x_i^-) - Z_{oi}], \tag{7}$$

and

$$Z(x_{i-1}^+) = Z_{oi}[I + H_i\Gamma_i H_i][I - H_i\Gamma_i H_i]^{-1}, \tag{8}$$

where Z_{oi} and H_i are the characteristic impedance matrix and the phase matrix of the ith step discontinuity; their elements are defined as

$$(Z_{oi})_{mn} = \delta_{mn}Z_{oin}, \tag{9}$$

$$(H_{oi})_{mn} = \delta_{mn}\exp(-j\kappa_{xin}l_i) \tag{10}$$

where κ_{xin} and Z_{oin} are, respectively, the wave number in the x direction and the characteristic impedance for the nth mode in the ith dielectric waveguide section with length l_i. It is obvious that the staircase approximation is very simple, and can be generally applied to nonuniform integrated optical devices with any profiles.

NUMERICAL RESULTS

To illustrate the electromagnetic scattering characteristics of nonuniform periodic structures, we present the following results. Consider the first case of a parallel-plate waveguide filled with a concave Bragg grating, shown in Figure 1(a). The profile of the concave grating region is characterized by a circle. We assume that each uniform dielectric waveguide region of the grating supports only the TE_0 guided mode. For the mode-matching procedures, the number of modes (M), including propagating and evanescent modes, has been set at 15 throughout this article for numerical analysis. Figure 1(c) shows the normalized reflection and transmission power as a function of wavelength λ for the structure of a parallel-plate waveguide filled with a concave Bragg grating, as shown in Figure 1(a) with $N = 20$ periods. The results show that there exist a main stop band and a series of tapered-intensity side lobes extending to smaller λ. We find, if the radius of curvature of the concave region is large enough, that the central frequency of the main stop band can be roughly

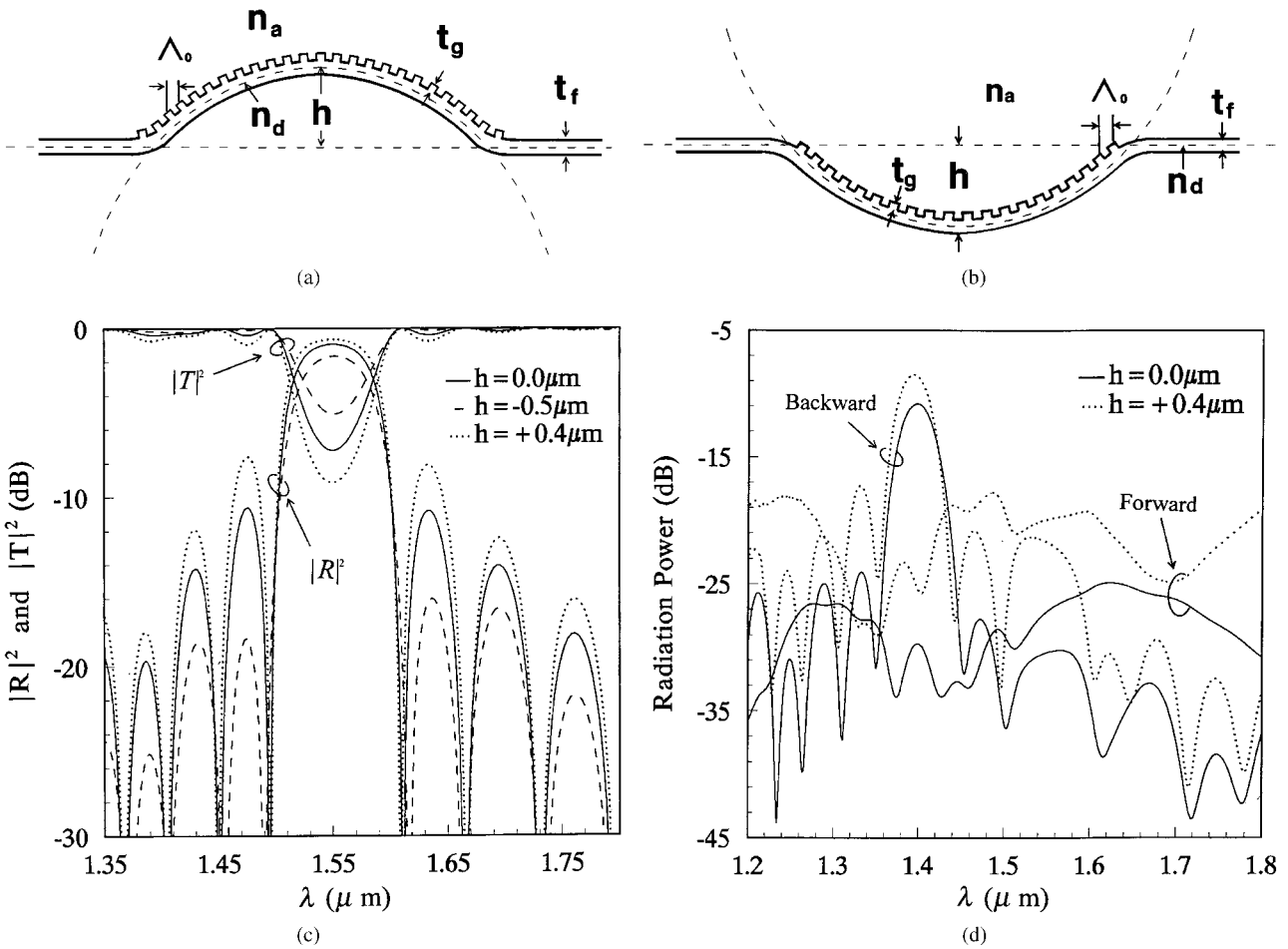

Figure 2 (a) Structure configuration of a Bragg grating bent upward along the parabola. (b) Structure configuration of a Bragg grating bent downward along with parabola. (c) Reflection and transmission spectrum of the fundamental TE mode of bent waveguide gratings bending with parabola curves: $n_d = 1.5$, $n_a = 1.0$, $t_f = 0.36$ μm, $t_g = 0.14$ μm, $\Lambda_0 = 0.6232$ μm and 25 periods. (d) Comparison of the variation of backward and forward radiation between uniform grating and upward bent waveguide grating

estimated from the uniform-grating Bragg condition, and that there exists a wide passband below $\lambda = 0.97$ cm.

In order to analyze open types of nonuniform periodic structures for integrated optics applications with the method presented here, we extend the two metal plates [Figure 1(a)] upwards and downwards, respectively, so as to minimize the effect on the grating caused by these plates. We preserve the metal plates in order to reduce the continuous spectrum of radiation modes into a complete set of discrete modes, as is customarily done in the literature [5]. Thus, part of the power of the TE_0 surface mode, which by scattering at the discontinuities of the open-type waveguide grating is coupled into the higher-order modes, can be viewed as the radiation associated with the continuous spectrum. The open nonuniform periodic gratings analyzed here are bent-waveguide-type gratings. The examples that we will discuss first are Bragg waveguide gratings bent into a parabolic shape, as shown in Figures 2(a) and 2(b). We use the notation $+h$ for the displacement of the top point of the upward parabola waveguide grating above the horizontal direction of the input/output waveguide shown in Figure 2(a); $-h$ represents displacement of the bottom of the downward-bent waveguide grating shown in Figure 2(b). The numerical results for the two types of bending are compared to that of the flat one in Figure 2(c). Apparently, if the value of $|h|$ increases gradually and the grating is bent more severely, the side lobes of the reflection spectrum decrease for a downward-bent waveguide grating, whereas an upward-bent grating shows the opposite

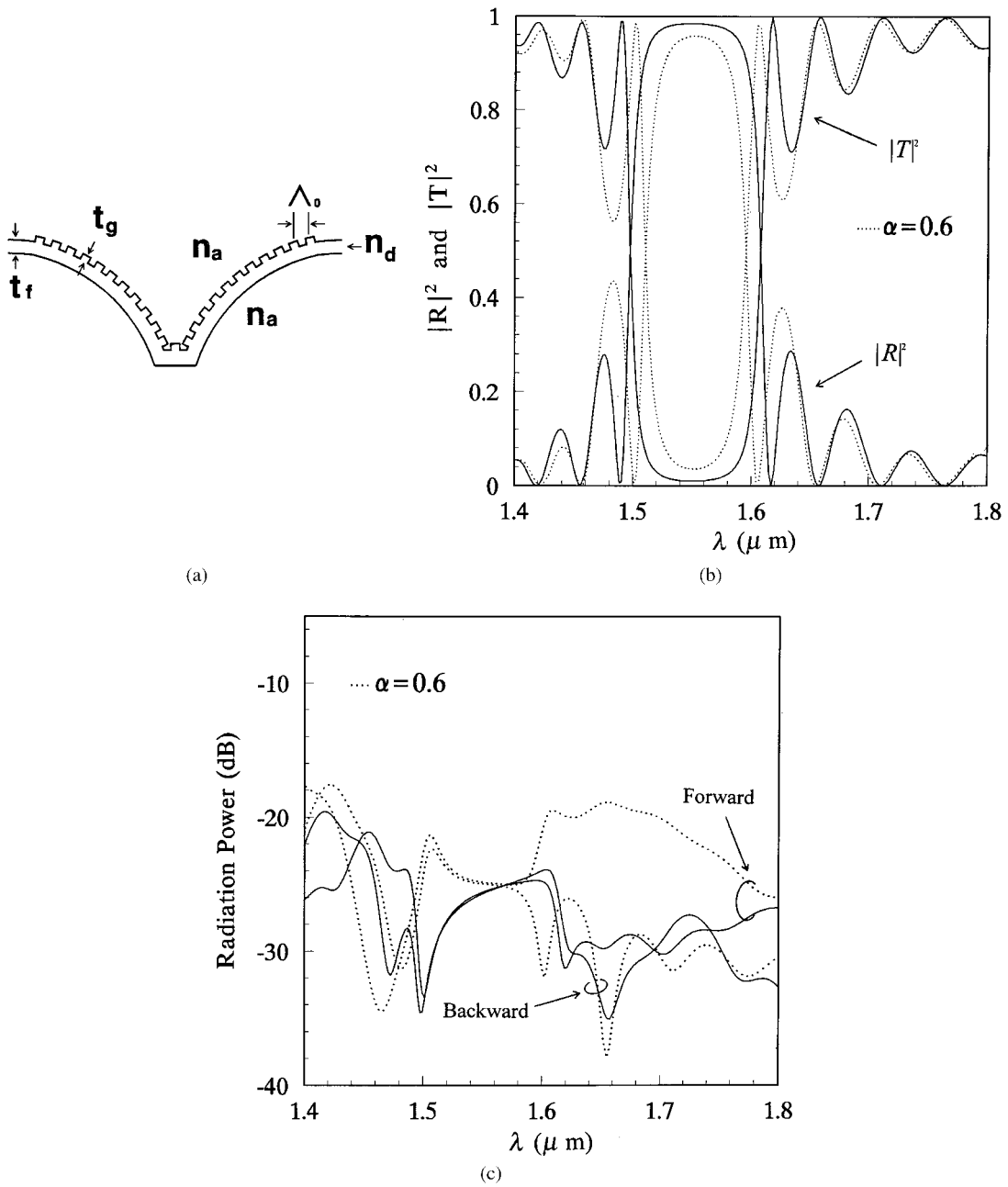

Figure 3 (a) Structure configuration of a bent waveguide grating with a twist and bending along with $y(x) = e^{-\alpha x}$ symmetrically. (b) Reflection and transmission spectrum as a function of λ for the structure of (a): $n_d = 3.4$, $n_a = 1.0$, $t_f = 0.15$ μm, $t_g = 0.06$ μm, $\Lambda_0 = 0.304$ μm, and 25 periodics. (c) Comparison of the variation of backward and forward radiation between uniform grating and bent waveguide grating for the structure of Figure 3(a)

effect. The bandwidth of the stop band changed slightly. For the downward parabolic bending of the grating, the side lobes are reduced, so part of the energy (depending on the structure parameters and incident wavelength λ) will be released as radiation loss. Figure 2(d) shows the comparison of the backward and forward radiation powers between the straight and bent waveguide gratings. The forward radiation means that the energy is radiated from grating in the same lateral direction as the incident wave, and the backward radiation is in the opposite direction. For uniform waveguide grating, there exists a backward leaky wave in the range of $\lambda = 1.3-1.42$ μm. The existence of the leaky region arises from the periodic nature of the grating waveguide; this has been pointed out in the literature [6]. The guided-wave scattering by the finite periodic discontinuities of grating will lead to more energy leakage into the air region if the average propagation constant β_d in the waveguide grating satisfies the inequality

$$k_a \geq \beta_\nu = \beta_d + (2\nu\pi/\Lambda_0), \qquad \nu = 0, \pm 1, \pm 2 \cdots \quad (1)$$

where k_a is the propagation constant in air and Λ_0 is the grating periodicity. For the leaky-wave region indicated in Figure 2(d), the only value that could satisfy the leakage condiction (11) is $\nu = -1$. In this case, β_{-1} is negative, so that the field scattered in the air region is inclined toward the $-x$ direction. The nonuniformity of the guiding structure also leads to more radiation loss into exterior region. Therefore, the radiation loss in the leaky-wave region will increase by bending the waveguide grating upward. Thus, the bent waveguide grating mentioned above has some advantages: For an upward-bending grating the radiation loss in the leaky-wave region will increase and may enhance the performance of a leaky-wave antenna. For a downward-bending grating, side lobes will be more efficiently suppressed and the grating can be used as a distributed feedback reflector. These conclusions hold also for optical material of a higher refraction index (for example, $n_d = 2.0$, 3.4, and so on). Besides, if there exists a drastic twist at the bottom of the bent waveguide grating, such as indicated in Figure 3(a), the reflection and transmission coefficient will also be affected. Such a twist may occur in waveguide grating because of a manufacturing imperfection. The waveguide grating under discussion bends down to and then up from its minimum, with the bend having an exponential profile. Figure 3(b) shows the normalized reflection and transmission powers as a function of wavelength, and Figure 3(c) shows the forward and backward radiation powers. For comparison, we also present the data for the uniform grating, shown by solid lines in these two figures. The numerical results show that if there is a twist, the stop-band intensity drops somewhat, its bandwidth narrows, and the side lobes nearest the primary reflection peak will increase. It is also found that forward radiation will increase by bending the waveguide grating, as shown in Figure 3(a). In summary, an accurate analysis of the effects caused by nonuniform (i.e., bent) gratings can be used effectively to manipulate the electromagnetic scattering characteristics of these waveguide gratings. Nonuniformities in waveguide gratings may provide an extra degree of freedom in designing and improving the performance of devices.

CONCLUSION

We have analyzed five types of nonuniform Bragg gratings by staircase approximation. Numerical results show that scattering properties of these nonuniform Bragg gratings can be determined by the shape of the nonuniformities (such as bending functions). Therefore, these types of periodic structures may provide another degree of freedom to design waveguide gratings for millimeter-wave or optical-frequency application.

REFERENCES

1. H. Kogelnik and C. V. Shank, "Coupled-Wave Theory of Distributed Feedback Lasers," *J. Appl. Phys.*, Vol. 43, No. 5, 1972, pp. 2328–2335.
2. S. T. Peng, "Rigorous Formulation of Dielectric Grating Waveguides—General Case of Oblique Incidence," *J. Opt. Soc. Am. Ser. A*, Vol. 6, 1989, pp. 1869–1883.
3. S. J. Chung and Jiunn-Lang Chen, "A Modified Finite Element Method for Analysis of Finite Periodic Structures," *IEEE Trans. Microwave Theory Tech.*, Vol. MTT-42, July 1994, pp. 1561–1566.
4. R. Pregla and W. Yang, "Method of Line for Analysis of Multilayered Dielectric Waveguides with Bragg Gratings," *Electron Lett.*, Vol. 129, No. 22, 1993, pp. 1962–1963.
5. S. J. Xu, S. T. Peng, and F. K. Schwering, "Transition in Open Millimeter-Wave Waveguides," *IEE Proc. Pt. H*, Vol. 136, No. 6, 1989, pp. 487–491.
6. T. Tamir (Ed.), *Integrated Optics*, Springer-Verlag, Berlin, 1975, pp. 96–100.

CCC 0895-2477/97

DIPOLE ANTENNAS ON PHOTONIC BAND-GAP CRYSTALS — EXPERIMENT AND SIMULATION

M. M. Sigalas,[1] R. Biswas,[1] Q. Li,[1] D. Crouch,[2] W. Leung,[3] Russ Jacobs-Woodbury,[3] Brian Lough,[3] Sam Nielsen,[3] S. McCalmont,[3] G. Tuttle,[3] and K. M. Ho[3]

[1] Ames Laboratory
Microelectronics Research Center
Department of Physics and Astronomy
Iowa State University
Ames, Iowa 50011

[2] Hughes Electronic Corporation
AET Center
P.O. Box 1973
Rancho Cucamonga, California 91729

[3] Ames Laboratory
Microelectronics Research Center
Iowa State University
Ames, Iowa, 50011

Received 20 January 1997

ABSTRACT: *The radiation patterns of dipole antennas on three-dimensional photonic crystal substrates have been measured and calculated with the finite-difference–time-domain method. The photonic band-gap crystal behaves as a perfectly reflecting substrate, and all the dipole power is radiated into the air side when driven at frequencies in the stop band. The radiation pattern is found for different positions and orientations of the dipole antenna. Antenna configurations with desirable patterns are identified. © 1997 John Wiley & Sons, Inc.* Microwave Opt Technol Lett 15: 153–158, 1997.

Key words: *photonic band-gap materials; dipole antennas; finite-difference–time-domain calculations*